

Solidification Modeling and Microstructural Characterization of Alloy IN718 Deposited by Laser Engineered Net Shaping

J.N. DuPont¹, J.G. Nawrocki¹, and M.L. Griffith²

1. Department of Materials Science and Engineering, Lehigh University, Bethlehem, PA
2. Mechanical Engineering Department, Sandia National Laboratory, Albuquerque, NM

Abstract

Alloy IN718 deposited by the LENS process was characterized using light optical, and scanning and transmission electron microscopy techniques. The as-solidified microstructure contained primary γ -austenite cells with intercellular NbC and Laves phases. Underlying layer microstructures were not altered by the thermal cycles of subsequent passes. Dendrite tip modeling calculations provided a reasonable estimate of cell core compositions measured experimentally by analytical electron microscopy techniques and were used to demonstrate that dendrite tip undercooling was not significant under the deposition conditions employed. Preliminary guidelines on solidification conditions required to suppress microsegregation during LENS deposition of IN718 are provided from the modeling results. A solute redistribution model was employed, which accurately described the solidification reaction sequence and resultant phases present in the final microstructure.

Introduction

Fabrication of superalloy components via Laser Engineered Net Shaping (LENS) is being considered for a variety of applications in the aerospace and defense industries. In these applications, alloy composition and LENS processing parameters will control the microstructure and concomitant properties. In terms of processing parameters, the as-solidified microstructure of a given alloy will be controlled by the travel speed and beam power, which dictate the solidification velocity and temperature gradient, while subsequent solid state reactions will be governed by the thermal history induced from deposition of subsequent layers. In order to accurately model microstructural development of LENS components, it is necessary to know the relative importance of liquid-to-solid and solid-to-solid transformations in determining the final microstructure. In steels where the post solidification γ (austenite) \rightarrow α (ferrite) solid state transformation occurs and the diffusion rate of carbon and other alloying elements is relatively rapid, it has been shown [Ref. 1] that subsequent thermal cycles after the initial deposition induce significant microstructural modification via solid-to-solid transformations. In this case, accurate microstructural prediction requires both solidification and solid state transformation models. However, in Ni base superalloys such as IN718, the γ phase is stable after solidification and no post-solidification allotropic transformations occur [Ref. 2]. Although precipitation reactions can lead to the formation of γ' , γ'' , and δ phases, these reactions are generally slow due to the low diffusion rates of substitutional alloying elements in the FCC matrix [Ref. 3]. In this case, post solidification reactions under LENS processing conditions may be negligible, in which case only the liquid-to-solid transformation needs to be considered for estimating the microstructure after deposition. However, no experimental information is available to confirm this. In addition, the high solidification rates possible with the LENS process are often viewed as a means for reducing undesirable microsegregation that typically occurs during solidification of superalloys in other fabrication methods such as casting and welding. To this point, there has

been no detailed microstructural characterization conducted on LENS deposited IN718 to determine the extent to which microsegregation can be suppressed under typical deposition conditions. In this research, alloy IN718 was prepared by LENS deposition and characterized using scanning and transmission electron microscopy. The type of phases and distribution of alloying elements that existed between the last pass (which experienced no subsequent thermal cycles) and the underlying passes was compared in order to assess the influence of subsequent thermal cycles on the as-solidified microstructure.

Experimental Procedure

Alloy IN718 was deposited into single line wall builds that were approximately 25 mm wide and 100 mm high. The LENS processing parameters were set at a travel speed of 7.6 mm/s and a powder flow rate of 35.4 mm³/sec. Samples were then sectioned for microstructural analysis via light and electron microscopy. Samples for light optical microscopy (LOM) and scanning electron microscopy (SEM) were mounted and polished using standard metallographic techniques and electrolytically etched in 10% chromic acid (balance water) solution. A JEOL 6300 field emission gun SEM was used for imaging in the secondary electron mode. Thin foils for transmission electron microscopy (TEM) were prepared by polishing 3mm diameter disks to a thickness of approximately 50um and then ion milling to electron transparency. The SEM and TEM analysis was conducted on the last pass (which experienced no subsequent thermal cycles) and the fifth from last pass, which experienced four subsequent thermal cycles. Microhardness measurements were conducted using a Vickers indenter with a 200 gram load.

Results

Figure 1 contains LOM photomicrographs of the line builds, which shows the last seven passes. The bottom region of each pass contains a light colored area, but microhardness measurements (shown in Figure 1a) indicate there is no significant difference in hardness in any particular region of the sample. The microstructure exhibited a cellular/dendritic substructure with interdendritic secondary phases (Figure 1b). Figure 2 shows higher magnification SEM views of regions of the last pass and the fifth from last pass. The region of the last pass shows two secondary interdendritic phases with different morphologies – a small, equiaxed phase and larger, globular phase (Figure 2a). The fifth from last pass shows essentially identical results (Figure 2b). Figures 3 and 4 show TEM images and electron diffraction patterns of these phases. The small, equiaxed phase was identified as FCC (Ti,Nb)C (Figure 3), while the larger, globular phase was identified as an HCP A₂B Laves phase (A = Fe,Ni,Cr and B = Nb,Mo, Figure 4). These phases have also been observed in IN718 solidified under lower cooling rate conditions found in fusion welding [Ref. 2]. There is no significant difference in the type of phases present between the first and fifth from last passes. AEM compositional profiles were also acquired across these passes to measure the distribution of alloying elements across the cellular substructure. Typical examples of AEM line scans are shown in Figures 5 (last pass) and Figure 6 (fifth from last pass). In each case, the cell cores are depleted in Nb and Mo and slightly enriched in Cr and Fe. This indicates that Nb and Mo segregate to the liquid during solidification while Fe and Cr slightly segregate to the solid. These results also indicate that the solidification velocity used here is not high enough to suppress microsegregation in this alloy system.

Discussion

The microstructural characterization data indicates that there is no significant difference in microstructure between the last pass and underlying passes which have been exposed to subsequent thermal cycles. This suggests that the as-deposited microstructure of IN718 does not change significantly from the thermal cycles induced by subsequent depositions. It is generally known [Ref. 3] that as-cast IN718 will precipitate γ' , γ'' , and δ phases upon heating at elevated temperatures. However, the time required to precipitate these phases is on the order of six minutes at 870 °C, and the times required for precipitation increase significantly at lower temperatures. Thermocouple measurements previously conducted on LENS deposits [Ref. 1] have shown that the peak temperature decreases to ~ 850 °C approximately five layers below the weld pool. More importantly, the time above the peak temperature is extremely short. Thus, based on these considerations, it is expected that precipitation reactions would not occur during deposition, and this was confirmed by the TEM microstructural characterization data. This indicates that the as-deposited microstructure for this alloy can be estimated from solidification models alone.

The main objective of the microstructural modeling described here is to predict the type of phases that form during solidification and the solidification conditions (solidification velocity and temperature gradient) required to suppress microsegregation. One of the major advantages of LENS processing is the potential for minimizing concentrations gradients in the solid, which are often detrimental to mechanical properties and corrosion resistance [Ref. 4]. Under rapid solidification conditions encountered during laser deposition, there can be significant reduction in the cell tip radius and accumulation of solute in the liquid ahead of the solid/liquid interface. Each of these factors leads to dendrite tip undercooling and a concomitant enrichment of solute in the primary solid. However, the AEM data presented in Figures 5 and 6 indicate that microsegregation is still persistent under the current set of deposition conditions. The set of conditions needed to reduce microsegregation can be estimated based on the model presented by Kurz *et al* [Ref. 5], which is given by

$$V^2 \left[\frac{\pi^2 \Gamma}{P^2 D_l^2} \right] + V \left[\frac{m_l C_o (1-k) \xi}{D_l [1 - (1-k) I(P)]} \right] + G = 0 \quad (1)$$

$$\xi = 1 - \frac{2k}{[1 + (2\pi/P)^2]^{1/2} - 1 + 2k} \quad (2)$$

where V is the solidification velocity, Γ is the Gibbs-Thomson parameter, P is the Peclet number defined as $VR/2D_l$, (R is the cell tip radius, D_l is diffusivity of solute in the liquid), m_l is the liquidus slope, C_o is the nominal alloy composition, k is the distribution coefficient, G is the mean temperature gradient, k is the equilibrium distribution coefficient, and I(P) is the Ivantsov function. A numerical technique is required to solve equation (1). This model provides information on the cell radius and corresponding cell tip temperature, T_{tip} , as a function of solidification velocity and temperature gradient. Once the cell tip temperature is established, the cell tip composition, C_l^* , can be determined by

$$C_l^* = \frac{C_o}{1 - (1 - k)I(P)} \quad (3)$$

Once C_l^* is known, the cell core composition, C_{core} (which was also measured experimentally by AEM) can be determined from knowledge of the equilibrium distribution coefficient. Figure 7 shows the calculated variation in T_{tip} , C_l^* , and C_{core} as a function of solidification velocity for IN718. Following the work of Knorovsky *et al* [Ref. 2], IN718 was modeled as a γ -Nb binary system for these calculations. A temperature gradient of 500 °C/mm was used for the calculations based on previous thermal analysis data conducted on the LENS process [Ref. 6]. Material constants used for the calculations are shown in Table 1. The liquidus temperature for IN718 (i.e., in the absence of undercooling) is ~1360 °C [Ref. 2]. Note that the suppression in the dendrite tip temperature is not significant for this alloy under typical LENS solidification velocities (~ 2 – 10 mm/s). As a result, there is not a large increase in the cell tip composition. The AEM data measured at the cell cores is plotted in Figure 7c assuming that the travel speed of the heat source is equivalent to the solidification velocity. The solidification velocity will approximately reach the travel speed at the weld pool centerline and decrease towards zero at the edge of the weld pool. There is reasonable agreement among the calculated and measured data, providing validation on the accuracy of the calculations. These modeling results can also be used to provide information on the solidification conditions required to suppress microsegregation, i.e., to identify conditions in which C_{core} approaches C_o . Figure 7d shows a plot of C_{core}/C_o (this ratio is numerically equal to k , the distribution coefficient) as a function of solidification velocity. Note that rather high solidification velocities are needed in order to appreciably suppress microsegregation. These results show that effective suppression of microsegregation during LENS deposition requires careful consideration of the processing parameters, most notably the travel speed.

Table 1. Material parameter values used in dendrite tip calculations.

Parameter	Value	Reference
Γ (K-mm)	0.0002	9
D_l (mm ² /sec)	0.02	9
m_l (°C/wt% Nb)	-8.3	10
k (unitless)	0.48	2

Having established that dendrite tip undercooling is not large under the current set of deposition conditions, the solute redistribution stage of solidification can be modeled by the approach previously presented by DuPont *et al* [Ref. 7]. The primary solidification path is given by

$$C_{l,Nb} = C_{o,Nb} \left[\frac{C_{o,C} - k_C C_{l,C}}{(1 - k_C) C_{l,C}} \right]^{k_{Nb} - 1} \quad (4)$$

Where $C_{l,Nb}$ and $C_{l,C}$ are the Nb and C concentrations in the liquid during the primary $L \rightarrow \gamma$ reaction, $C_{o,Nb}$ and $C_{o,C}$ are the nominal Nb and C concentrations, and k_{Nb} and k_C are the distribution coefficients for Nb and C. A liquidus projection is needed along with the solidification path calculation in order to determine the solidification reaction sequence and

concomitant phases present after solidification. Figure 8 shows the solidification path (according to eq. 4) superimposed on a pseudo-ternary liquidus projection for IN718 that was calculated with Thermo-Calc thermodynamic system [Ref. 8] . These results indicate that solidification starts by a $L \rightarrow \gamma$ reaction, which rejects Nb and C to the intercellular liquid. This process continues until the primary solidification path intersects the NbC/ γ two fold saturation line, at which point γ and NbC start forming simultaneously from the liquid. This process continues as the liquid composition follows the NbC/ γ two fold saturation line until the NbC/ γ /Laves Type II reaction is reached, at which point γ and Laves form as solidification goes to completion. This predicted reaction sequence is in agreement with the NbC and Laves phases observed during microstructural characterization. These results do not account for the presence of cell tip undercooling, since it was previously demonstrated to be negligible under the current set of deposition conditions. However, process optimization studies are underway in order to identify parameters, which induce significant cell tip undercooling and reduce microsegregation. In this case, dendrite tip undercooling calculations must be combined with solute redistribution computations for accurate modeling. This work is currently underway.

Conclusions

Alloy IN718 deposited with the LENS process solidifies by a three step reaction sequence; $L \rightarrow \gamma$, followed by $L \rightarrow (\gamma + \text{NbC})$ and $L \rightarrow (\gamma + \text{Laves})$. This solidification reaction sequence has been accurately modeled by solute redistribution calculations and the use of a computed pseudo-ternary liquidus projection. Thermal cycles from deposition of subsequent layers have no significant effect on the as-solidified microstructure. Under low travel speed conditions, dendrite tip undercooling is not significant and microsegregation is not suppressed. Dendrite tip undercooling models have been used to estimate solidification velocities required to minimize microsegregation.

Acknowledgements

Prof. DuPont gratefully acknowledges support of this work by the National Science Foundation through a PECASE Award, Grant No. DMI 9983968, made through the Division of Manufacturing and Industrial Innovation and helpful discussions with Dr. Delcie Durham of NSF. The portion of research conducted at Sandia National Laboratory was supported by the U. S. Department of Energy under contract DE-AC04-94AL85000. Sandia is a multiprogram laboratory operated by Sandia Corporation, a Lockheed Martin Company, for the United States Department of Energy.

References

1. M.L. Griffith, M.E. Schlienger, L.D. Harwell, *Materials and Design*, Vol. 20, 1999, pp. 107-113.
2. Knorovsky, G.A., Cieslak, M.J., Headley, T.J., Romig, Jr., A.D., and W.F. Hammett, *Metallurgical Transactions A*, Vol. 20A, 1989, pp. 2149-2158.
3. A. Oradei-Basile and J.F. Radavich, *Superalloys 718, 625, and Various Derivatives*, TMS, 1991, pp. 325-334.
4. K.R. Luer, J.N. DuPont, A.R. Marder, and C.K. Skelonis, Corrosion Fatigue of Alloy 625 Weld Claddings Exposed to Combustion Environments, *Materials at High Temperatures*, Vol. 18, 2001, pp. 11-19.
5. W. Kurz, B. Giovanola, and R. Trivedi, *Acta Materialia*, Vol. 34, 1986, pp. 823-830.

6. W. Hofmeister, M. Wert, J. Smugeresky, J.A. Phillipier, M. Griffith, and M. Ensz, *JOM*, Vol. 51, 1999, (e-journal version).
7. DuPont, J.N., Robino, C.V., and A.R. Marder, *Acta Materialia*, Vol. 46, no. 13, 1998, pp. 4781-4790.
8. Saunders, N. *Ni-Data v.3*, Thermotech Ltd., Surrey Technology Centre, The Surrey Research Park Guildford, Surrey GU2 5YG, U.K.
9. W. Kurz and D.J. Fisher, *Fundamentals of Solidification*, 3rd Ed., Trans Tech Publications, 1989.
10. J.N. DuPont, C.V. Robino, and A.R. Marder, Modeling Mushy Zones in Welds of Multi-Component Alloys: Implications to Solidification Cracking, *Science and Technology of Welding and Joining*, 1999, Vol. 4, No. 1, pp. 1-14.

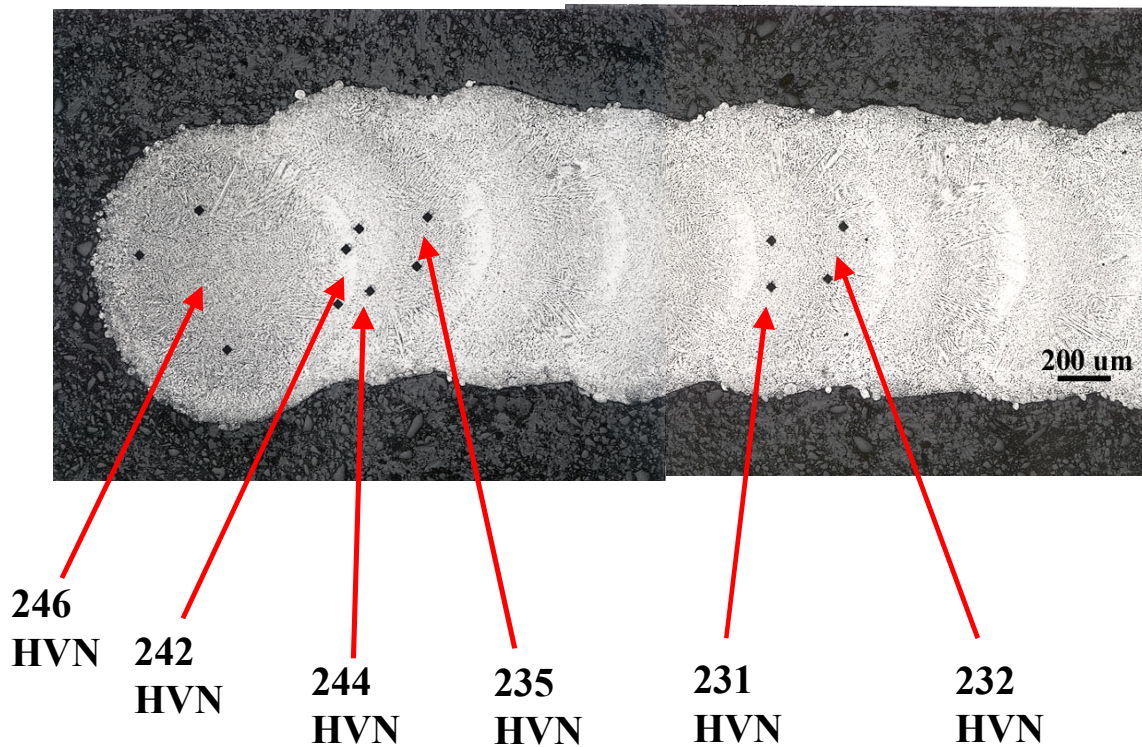


Figure 1a: Macrostructure and hardness of an IN718 LENS deposit.

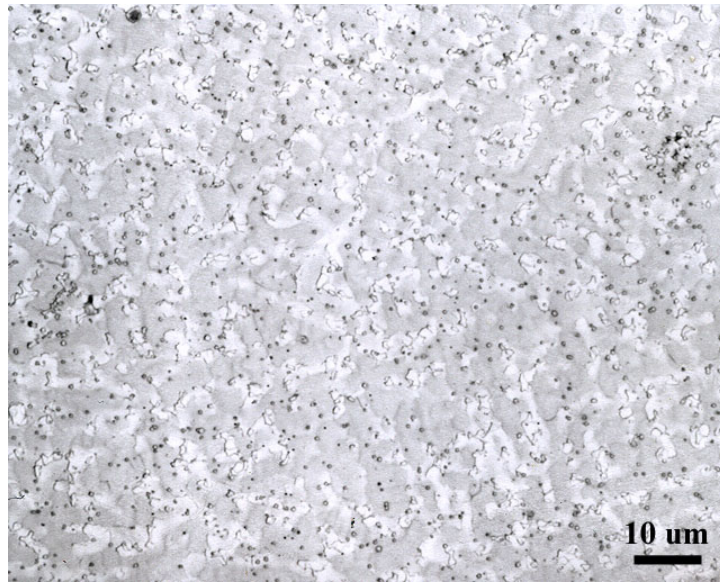
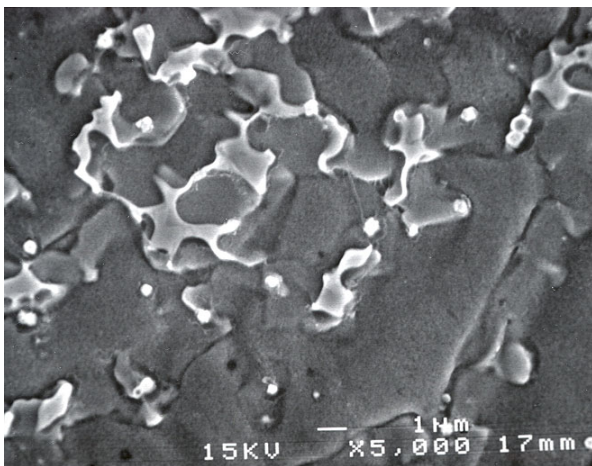
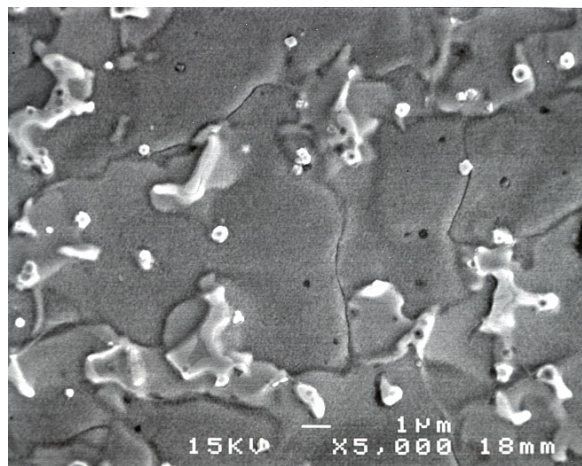


Figure 1b: Representative LOM photomicrograph of an IN718 line build showing a cellular/dendritic substructure and interdendritic secondary phases.



a



b

Figure 2: SEM photomicrographs of (a) the last pass and (b) the fifth from last pass of an IN718 line build.

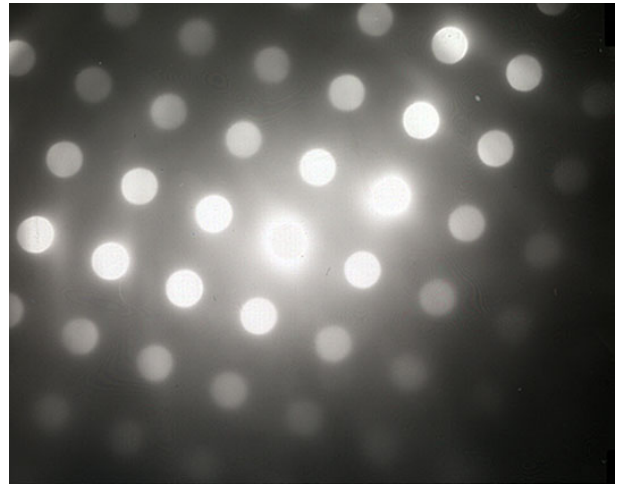
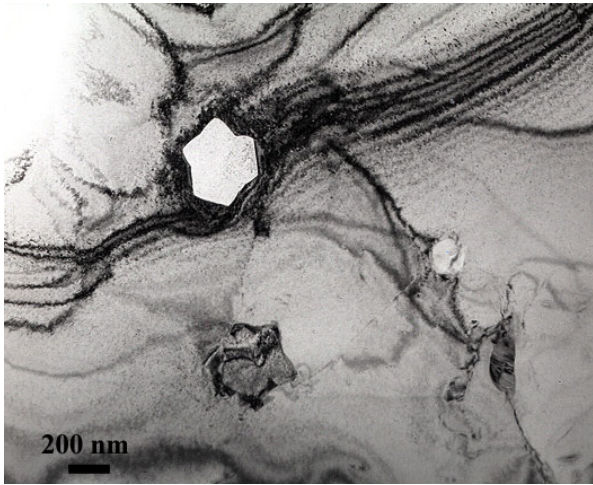


Figure 3: TEM photomicrograph of FCC (Ti,Nb)C and accompanying electron diffraction pattern showing a [011] zone axis.

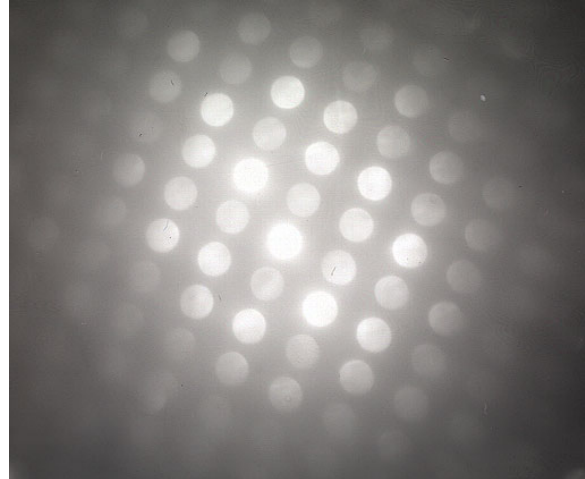
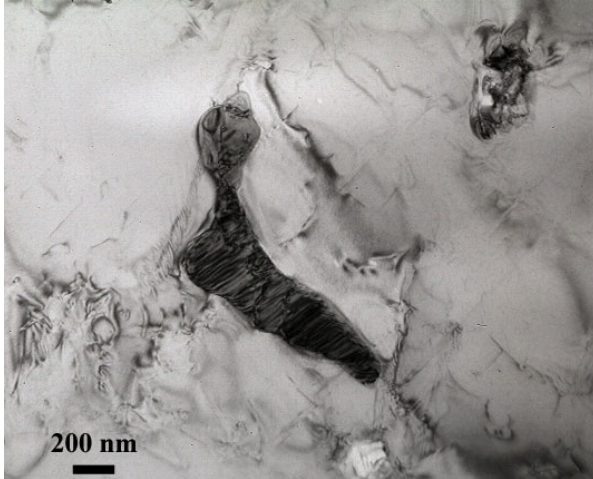


Figure 4: TEM photomicrograph of HCP A₂B Laves phase (A=Fe,Ni,Cr and B= Nb,Mo) and accompanying electron diffraction pattern showing a [311] zone axis.

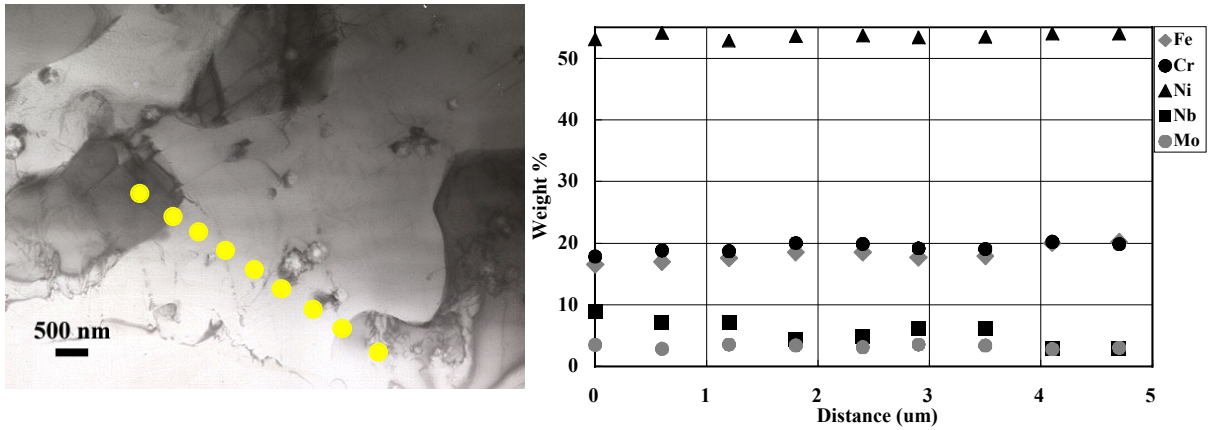


Figure 5: Typical AEM line scan of the last pass in an IN718 line build indicating Nb and Mo segregation. The points shown on the micrograph from the upper left to the lower right correspond to increasing distance on the accompanying graph.

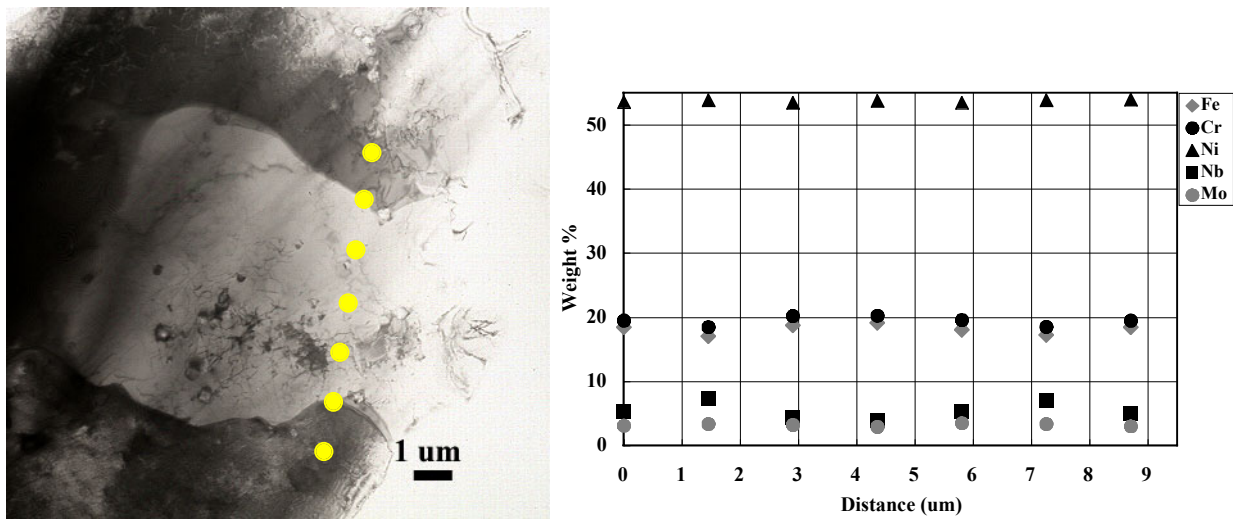


Figure 6: Typical AEM line scan of the fifth pass in an IN718 line build indicating Nb and Mo segregation. The points shown on the micrograph from the bottom to top correspond to increasing distance on the accompanying graph.

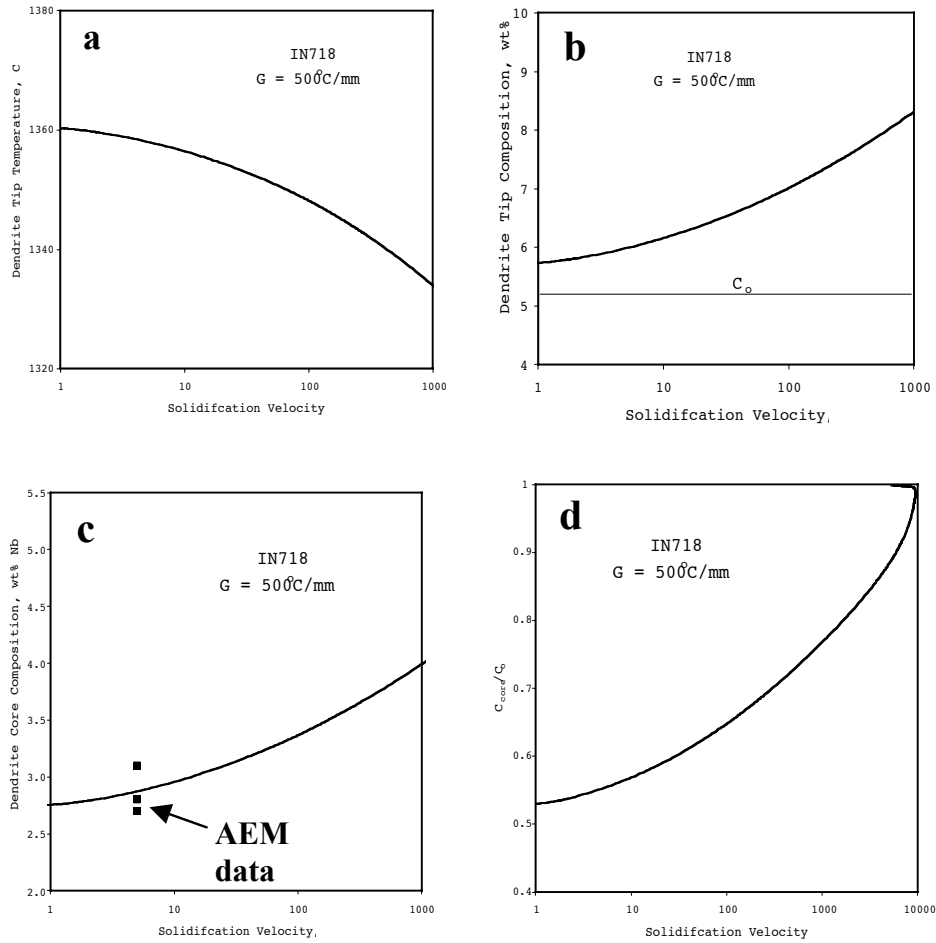


Figure 7. Dendrite tip calculations. a) Dendrite tip temperature as a function of solidification velocity, b) Dendrite tip composition as a function of solidification velocity, c) Dendrite core composition as a function of solidification velocity with AEM data plotted, d) C_{core}/C_0 as a function of solidification velocity.

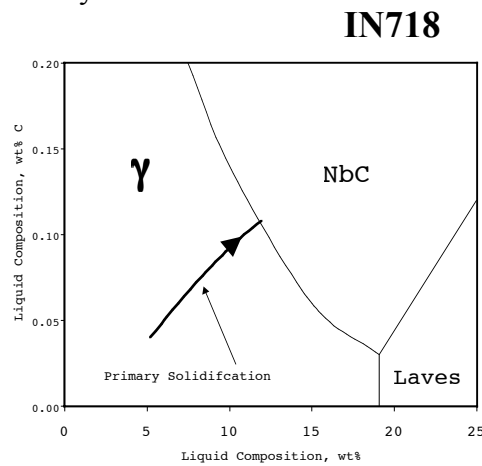


Figure 8. Calculated primary solidification (equation (4)) superimposed on the IN718 pseudo ternary liquidus projection.